JOURNAL OF CATALYSIS **167,** 92–105 (1997)
ARTICLE NO. CA971554

A Novel Process for the Preparation of Cu/ZnO and Cu/ZnO/Al_2O_3 Ultrafine Catalyst: Structure, Surface Properties, and Activity for Methanol Synthesis from $CO_2 + H_2$

Qi Sun,* Yu-Long Zhang,* Hai-Ying Chen,* Jing-Fa Deng,*,[1] Dong Wu,† and Song-Ying Chen†

*Chemistry Department, Fudan University, Shanghai, 200433, People's Republic of China; and †Institute of Coal Chemistry, Academia Sinica, P.O. Box 165, Taiyuan, Shanxi, People's Republic of China

Received April 8, 1996; accepted December 3, 1996

Cu/ZnO and Cu/ZnO/Al_2O_3 ultrafine particle catalysts have been prepared by a novel oxalate gel coprecipitation method. XRD, TEM, TG/DTG, and EXAFS were used to characterize the phases, morphology, and particle sizes of the precursors of the catalysts and reduced catalysts. The results showed that isomorphous substitution took place between copper and zinc in the precipitates. The addition of Al to the binary system made the copper and zinc in the catalyst exist in much smaller crystallites and exhibit an amorphous-like structure. The effects of composition, structure, and surface property of the catalysts as well as the reaction condition on the activity and selectivity to methanol for methanol synthesis from $CO_2 + H_2$ were investigated. The activity was found to increase with the increase of surface area of metallic copper in the range of 10–60% of copper content, but it decreased as the copper content exceeded 60%, although the metallic copper surface area was higher. This was explained by the strong synergy between copper and zinc oxide. The effect of contact time on the relative selectivity ($\gamma = S_{CH_3OH}/S_{CO}$) and selectivity of methanol was also investigated. The results indicated that methanol was formed directly from hydrogenation of CO_2.

INTRODUCTION

Methanol synthesis from syngas has been an important chemical process since the invention of a high-pressure method by BASF in 1920s (1, 2). The low-pressure process for synthesis of methanol using Cu/ZnO/Al_2O_3 catalyst was investigated by ICI in the late 1960s (3, 4). A high catalytic activity of the catalyst employed in their work was observed at 5–10 MPa and 230–300°C. However, it was reported that the composition of feed gas had a significant effect on the productivity and selectivity of methanol (5–13). Klier *et al.* (7, 14) studied the influence of carbon dioxide on the activity of Cu/ZnO catalyst and observed a maximum synthesis rate at CO_2/CO ratio of 1/14. By isotopic studies using C^{13} or other methods, some authors (6–8, 10, 15–18) have confirmed that methanol was mainly formed from CO_2 rather than CO in the hydrogenation of the mixture of CO and CO_2. Since the rate of CO_2 hydrogenation to methanol was much greater than the rate of CO hydrogenation, CO_2 was the main direct carbon source of methanol synthesis. On the other hand, Chanchlani *et al.* (19) have measured the formation rates of methanol at different synthesis gas compositions and reaction temperatures; the results indicated that methanol could be formed from either CO or CO_2. When both reactants were present in the syngas, the rates from either reactant were additive, with a further contribution to methanol arising from interconversion, mainly CO to CO_2, via the water–gas shift, utilizing water formed in the methanol synthesis. At temperatures lower than 250°C, methanol synthesis rates exhibited monotonical increase with increasing CO_2 concentration, while a maximum rate was observed at higher temperatures. This observation was interpreted as being due to a change in the importance of CO and CO_2 as the source of methanol in the synthesis. However, Vedage *et al.* (20) concluded that CO was the dominant reactant for producing methanol, while CO_2 was a minor reactant. In spite of this rather convincing evidence, the controversies for the direct carbon source of methanol synthesis have not yet been completely settled.

Recently, the effective utilization of CO_2 has been catching great attention due to its environmental relevance. In addition, synthesis of methanol from $CO_2 + H_2$ is one of the most economic processes. However, Inui *et al.* (21) reported that the activity was very low when the commercial Cu/ZnO/Al_2O_3 catalyst was used in the process of methanol synthesis from $CO_2 + H_2$. Therefore, it is important to synthesize and develop new catalysts with a higher activity and better selectivity to methanol.

However, many studies have been focused on the structure of the active surface, the nature of the active sites, and the reaction mechanism. It was suggested that the active centers for methanol synthesis were Cu–Zn pair (14, 22), Cu^+ ions (7, 13, 23–28), Cu^0–Cu^+ (11, 29–32), or copper metal (30, 31, 33, 34). But it was also found that, in all

[1] To whom correspondence should be addressed.

0021-9517/97 $25.00

cases, the methanol productivity of the individual metals or oxides were of some orders of magnitude lower than the metal/oxide combination. The explanation for this remarkable synergy has remained controversial. Klier (14) proposed that the active site was the partly oxidized copper dissolved in the ZnO lattice. Herman *et al.* (13) suggested that the methanol synthesis activity could be attributed to the concentration of Cu^+ dissolved in ZnO. Frost (35) proposed that the interaction between small particles and an encapsulating oxide would give rise to an increase in the concentration of surface oxygen vacancies, which were regarded to be the active sites for methanol synthesis.

In this work, a novel process for the preparation of $Cu/Zn/Al_2O_3$ ultrafine catalysts by means of gel-coprecipitation of oxalates was utilized. These catalysts showed higher catalytic activity for the synthesis of methanol from $CO_2 + H_2$. The structure and morphology of the precipitates and their calcined and reduced forms were studied by transmission electron microscopy (TEM), X-ray diffraction (XRD), thermogravimetry and differential thermogravimetry (TG/DTG), N_2O-decomposition adsorption, and extended X-ray adsorption fine structure (EXAFS). The effects of composition, structure, surface property of the catalysts, and reaction condition on the activity and selectivity of methanol for methanol synthesis from $CO_2 + H_2$ were investigated.

EXPERIMENTAL

Preparation of Catalysts

Cu/ZnO and $Cu/ZnO/Al_2O_3$ catalysts with various compositions used in this study were prepared by an oxalate gel coprecipitation method similar to that described previously (36). The mixed nitrates and 20% excess of oxalic acid were dissolved in ethanol (provided by Shanghai Chemical Reagent Institute, $\geq$99.7%), individually. The two solutions were mixed at room temperature with vigorous stirring. The precipitates were formed and separated by centrifuge and then dried at 110°C overnight. The volume of the precipitates shrank to less than 1/5 of their original volume after drying. Obviously the precipitates showed gel-like properties. This novel method was designated as oxalate gel coprecipitation. Some catalysts were also prepared by a conventional method, in which the mixed aqueous solution of copper nitrate, zinc nitrate, and aluminum nitrate (each 0.1 *M*) was precipitated by aqueous solution of oxalic acid (0.1 *M*) at room temperature with vigorous stirring. However, the volume of the precipitates did not shrink during the drying process. This was referred to as conventional oxalate coprecipitation method. The precipitates of oxalates were calcined in a muffle oven at 150°C for 1 h, 200°C for 1 h, 250°C for 1 h, 300°C for 1 h, and 360°C for 4 h. Subsequently, the ultrafine particles of CuO/ZnO and $CuO/ZnO/Al_2O_3$ catalysts were obtained.

Catalyst Characterization

XRD determination was recorded using a Rigaku, Dmax-rA X-ray powder diffractometer with Cu$K\alpha$ radiation, graphite monochromator. The mean crystallite size was calculated using Scherrer equation from half-width of the diffraction lines of Cu(111) and ZnO(100). The TEM micrographs were obtained with a Hitachi H600 scantransmission electron microscope. Thermogravimetric and differential thermogravimetric analyses were carried out in the air with a heating rate of $5°C \cdot min^{-1}$ using a Dupont-951 thermal gravimetric analyzer. The specific surface area of metallic copper was measured by the decomposition of N_2O (20, 37–39) on the surface of metallic copper as follows: $2Cu + N_2O = N_2 + (Cu{-}O{-}Cu)_s$. The pulse titration technique was employed in our experiment. N_2 was used as the carrier gas and a thermal conduct detector was used to detect the amount of the consumption of N_2O. The specific area of metallic copper was calculated from the total amount of N_2O consumption with $1.46 \times 10^{19} \cdot m^{-2}$ Cu (37, 39). The accuracy of the metallic copper surface area measurement was higher than 95%.

XAFS spectra of both Cu and Zn *K*-edges were recorded on the BL-10B in the National Laboratory of High Energy Physics (KEK, Tsakuba). The electron beam energy of the storage ring was 2.5 GeV and the stored current was in the range of 360–260 mA. The monochromator was channel-cut Si(311). The energy calibration was monitored using Cu foil and was set at 89803 eV at the *K* absorption edge. Data were collected in the transmission mode using ion chambers at room temperature. The data analysis was conducted using the EXAFS analysis program EXAFS(II) (40).

Measurement of Catalytic Activity

The catalytic activity was tested in a pressurized continuous tubular flow fixed-bed microreactor as described previously (36). The catalyst (40–60 mesh, 0.5 ml) was packed into a stainless-steel reactor (i.d., 6.0 mm) and reduced in flowing premixed H_2/Ar(5/95) flow of $40 \text{ ml} \cdot \text{min}^{-1}$ (NTP). The temperature was increased to 250°C with a heating rate of $2°C \cdot min^{-1}$ and then kept at this temperature for 10 h. After reduction, the gas flow was switched to premixed CO_2/H_2(1/3). The reaction was carried out under a pressure of 2.0 MPa, a temperature in the range of 180 to 300°C, and at an hourly space velocity (SV) of 3,600 to 25,000 h^{-1}. Checks were made for heat and mass transport interference employing various criteria (for gradients of temperature and concentration with the catalyst and within the film surrounding it) proposed in the literature (41). All of these tests were strongly negative, indicating the absence of transport masking. From these calculations, particle sizes and gas flow rates at which masking would be eliminated were selected, and these conditions were used in the subsequent experiment. All experimental data were obtained

under steady-state conditions that were usually maintained for several hours before changing the reaction conditions to obtain another set of data. The products were analyzed by an on-line gas chromatograph with a thermal conductivity detector, in which two parallel connected columns, Porapak-Q and TDX-01, were used to separate reaction products.

RESULTS AND DISCUSSION

Structure of the Precipitates of Oxalate

The XRD patterns of the precipitates prepared by the oxalate gel-coprecipitation are shown in Fig. 1. Only two phases (α-$ZnC_2O_4 \cdot 2H_2O$, $CuC_2O_4 \cdot xH_2O$) were observed in the patterns. No β-ZnC_2O_4 phase, which appeared in the conventional oxalate coprecipitation process (36), was detected. This indicates that the structure and morphology of the precipitates formed by the novel process is different from the precipitates formed by the conventional process. It can also be seen from Fig. 1 that the proportion of α-$ZnC_2O_4 \cdot 2H_2O$ to $CuC_2O_4 \cdot xH_2O$ varied with the change of molar ratio of Cu to Zn. The fraction of α-$ZnC_2O_4 \cdot 2H_2O$ decreased with the decrease of Zn content. When Cu/Zn = 1, the peak of $CuC_2O_4 \cdot xH_2O$ was much stronger than that of $ZnC_2O_4 \cdot 2H_2O$, when Cu/Zn = 2, only the diffraction line of $CuC_2O_4 \cdot xH_2O$ was observed. This indicates that a single-phase precipitate was formed and a considerable amount of the zinc was incorporated in the structure of $CuC_2O_4 \cdot xH_2O$ by isomorphous substitution between copper and zinc under such conditions.

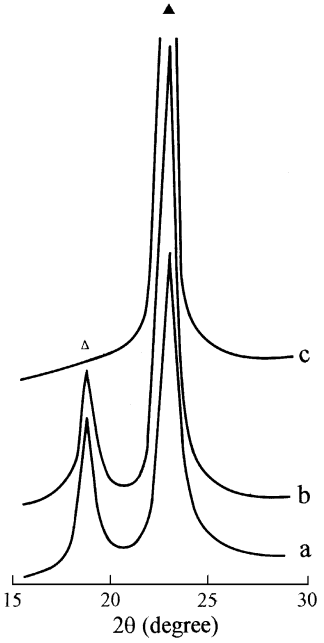

FIG. 1. XRD patterns of the gel oxalate precipitates with various compositions. (a) CZA02 (Cu/Zn/Al = 30/60/10); (b) CZA03 (Cu/Zn/Al = 45/45/10); (c) CZA04 (Cu/Zn/Al = 60/30/10). (▲) $CuC_2O_4 \cdot xH_2O$; (△) α-$ZnC_2O_4 \cdot 2H_2O$.

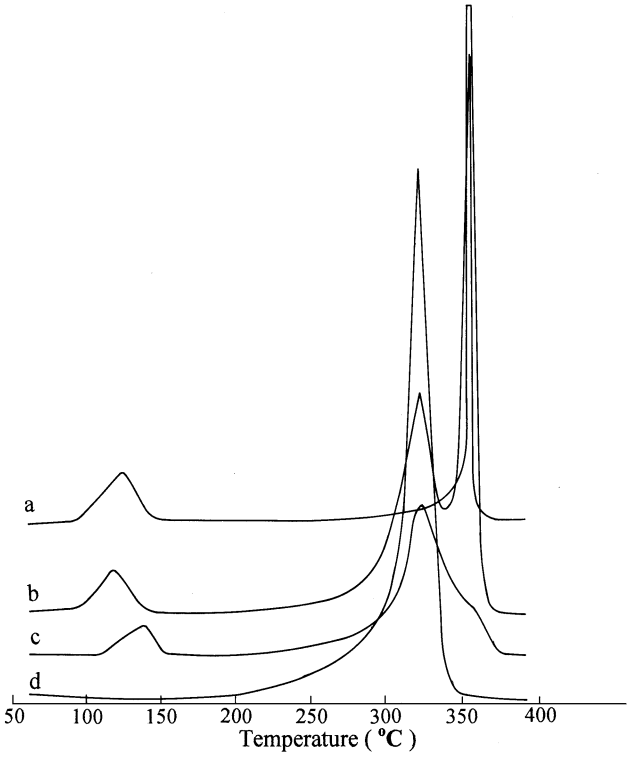

FIG. 2. DTG of the gel oxalate precipitates with various compositions. (a) CZA01 (Cu/Zn/Al = 10/80/10); (b) CZA02 (Cu/Zn/Al = 30/60/10); (c) CZA03 (Cu/Zn/Al = 45/45/10); (d) CZA04 (Cu/Zn/Al = 60/30/10).

The isomorphous substitution of zinc and copper in the catalyst precursor was further demonstrated by the TG/DTG analysis of the oxalate precipitates having various compositions. In DTG spectra shown in Fig. 2, three peaks for the loss of weight were observed at 110, 322, and 358°C. The peak at about 110°C was due to the desorption of physically absorbed water. The peaks at 322 and 358°C were ascribed to the decomposition of oxalate precipitates. We denote them as α(322°C) and β(358°C) peaks, respectively. With the increase of copper content, the α peak increased while the β peak decreased. Obviously, the α and β peaks could be assigned to the decomposition of CuC_2O_4 and ZnC_2O_4 phases, respectively. Only the β peak was observed when Cu/Zn $\leq$ 1/8, and only the α peak was observed at Cu/Zn $\geq$ 2. This indicates that the precipitates were single phase under these two conditions. Namely, only the ZnC_2O_4 phase was formed at lower copper content and only the CuC_2O_4 phase was formed at higher copper content. This is consistent with the result from XRD. Table 1 lists the total loss of weight for decomposition of CuC_2O_4 and ZnC_2O_4 to CuO, ZnO (the desorption of physical absorbed water was not included), and fractions of the α, β peak. It can be seen that although total loss of weight was approximate to the theoretical loss of weight (meaning the loss of

TABLE 1

Results of DTG Analysis for the Precursors of the Catalysts with Various Compositions

Catalysts[a]	Composition (atom) Cu/Zn/Al	Loss of weight (%) Total	α	β
CZA01	10/80/10	49.7	0.0	49.7
CZA02	30/60/10	50.0	25.7	24.3
CZA03	45/45/10	49.9	41.6	8.3
CZA04	60/30/10	48.4	48.4	0.0
CZA05[b]	45/45/10	46.2	27.2	19.0

[a] The catalyst with Cu/Zn/Al = 10/80/10 was assigned as CZA01, Cu/Zn/Al = 30/60/10 as CZA02, Cu/Zn/Al = 45/45/10 as CZA03, Cu/Zn/Al = 60/30/10 as CZA04, and Cu/Zn/Al = 80/10/10 as CZA06 (in Table 3), respectively.

[b] Prepared by the conventional coprecipitation.

weight during the decomposition of CuC_2O_4 and ZnC_2O_4 to CuO and ZnO, i.e., $Cu(C_2O_4)$ or $Zn(C_2O_4)$=CuO or $ZnO + CO\uparrow + CO_2\uparrow$, the theoretical loss of weight equaling $(M_{CO} + M_{CO_2})/M_{Cu(or\ Zn)C_2O_4}$ (here M is molar mass)), there was a remarkable disparity between the fraction of the α, β peaks and the composition of the precursors of the catalysts. This reveals the degree of isomorphous substitution between copper and zinc to some extent.

Figure 3 shows the DTG spectra of the precipitates with Cu/Zn/Al = 45/45/10 prepared by both the conventional and the novel coprecipitation of oxalate. It can be seen that there was a great difference between the two kinds of precipitates. Although both the α and the β peaks were observed in both precipitates prepared by the conventional and the novel method, the intensity of the β peak for the precipitates prepared by the novel method decreased so rapidly that only a shoulder peak could be observed. This indicates that the fraction of ZnC_2O_4 structure in the precipitates prepared by the conventional method was much higher than that in the precipitates prepared by the novel method. The explanation for this can be attributed to the possibility that there was less zinc incorporated into the CuC_2O_4 phase during the former precipitation.

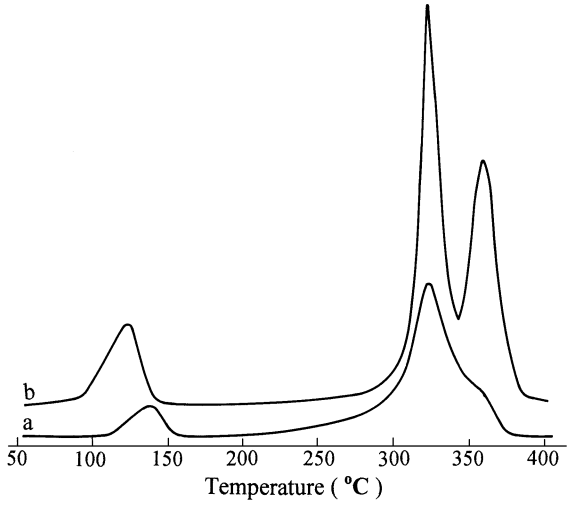

FIG. 3. DTG of the precursors before calcination for Cu : Zn : Al = 45 : 45 : 10. (a) Gel-precipitate prepared by the move gel oxalate coprecipitation method (CZA03); (b) crystal-precipitate prepared by the conventional oxalate coprecipitation method (CZA05).

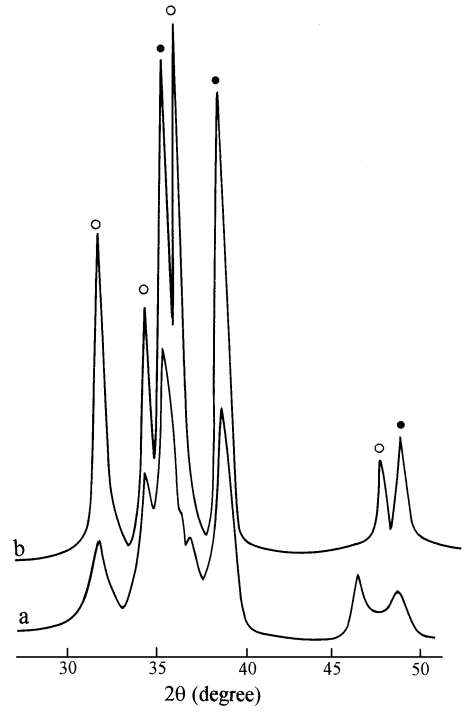

FIG. 4. XRD of the calcined CuO/ZnO and CuO/ZnO/Al_2O_3 catalysts. (a) CZA03 (Cu/Zn/Al = 45/45/10); (b) CZ02 (Cu/Zn = 50/50). (●) CuO; (○) ZnO.

Characterization of Calcined Catalyst

The XRD patterns for the binary (Cu/Zn = 50/50) and ternary (Cu/Zn/Al = 45/45/10) calcined catalysts (assigned as CZ02 and CZA03, respectively) prepared by the oxalate gel coprecipitation are shown in Fig. 4. The results indicate that copper and zinc were present in the CuO and ZnO phase in the calcined catalyst. This observation from XRD is consistent with the DTG results mentioned above. For the ternary catalyst, the diffraction peaks of ZnO and CuO were broadened remarkably and overlapped. Furthermore, no lines from an aluminum phase could be identified. In contrast to the ternary catalyst, the binary CuO/ZnO catalyst showed much narrower and sharper diffraction and a resolvable peak at $2\theta = 35.3^\circ$. The results show that the addition of Al_2O_3 had a significant influence on the particle size distribution and the structure of the catalyst. The copper, zinc, and aluminum phases were present in an amorphous-like or microcrystalline state in the ternary catalysts. The transmission electron micrographs of a binary catalyst (CZ02) with Cu/Zn = 1/1 and a ternary catalyst

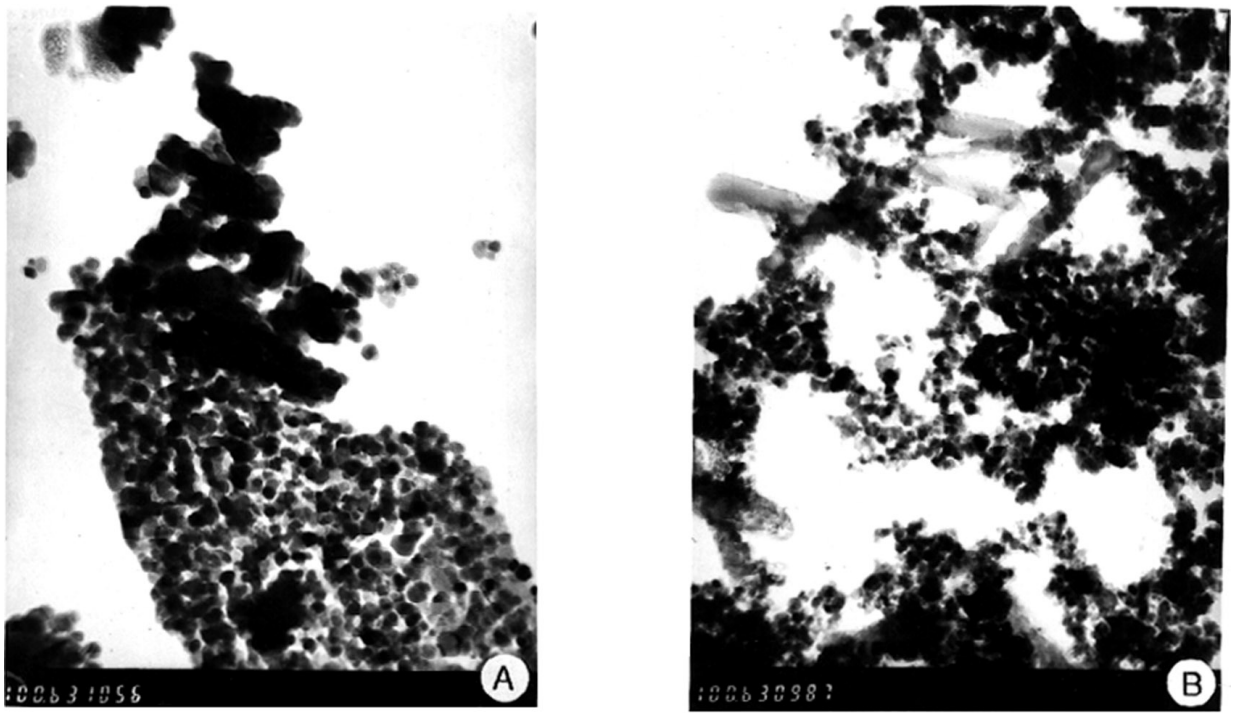

FIG. 5. TEM of the calcined binary and ternary catalyst. (A) CZ02 (Cu/Zn = 50/50); (B) CZA03 (Cu/Zn/Al = 45/45/10).

(CZA03) with Cu/Zn/Al = 45/45/10 are shown in Fig. 5. The morphology of the two calcined catalysts clearly demonstrates that the binary catalyst consisted of larger particles of similar shape, which often appeared in larger agglomerates, than the ternary catalyst did.

However, since the broadening of CuO and ZnO diffraction lines are due to their much finer particle size and the most intense ZnO diffraction line overlaps with the diffraction line from CuO phase (see Fig. 4), it is difficult to identify whether or not some copper species were substituted in the ZnO phase. In order to shed further light on this question, XAS (X-ray absorption spectroscopy) and EXAFS were employed. Figure 6A shows the Cu absorption *K*-edge for the calcined binary (CZ03) and ternary (CZA04) catalysts

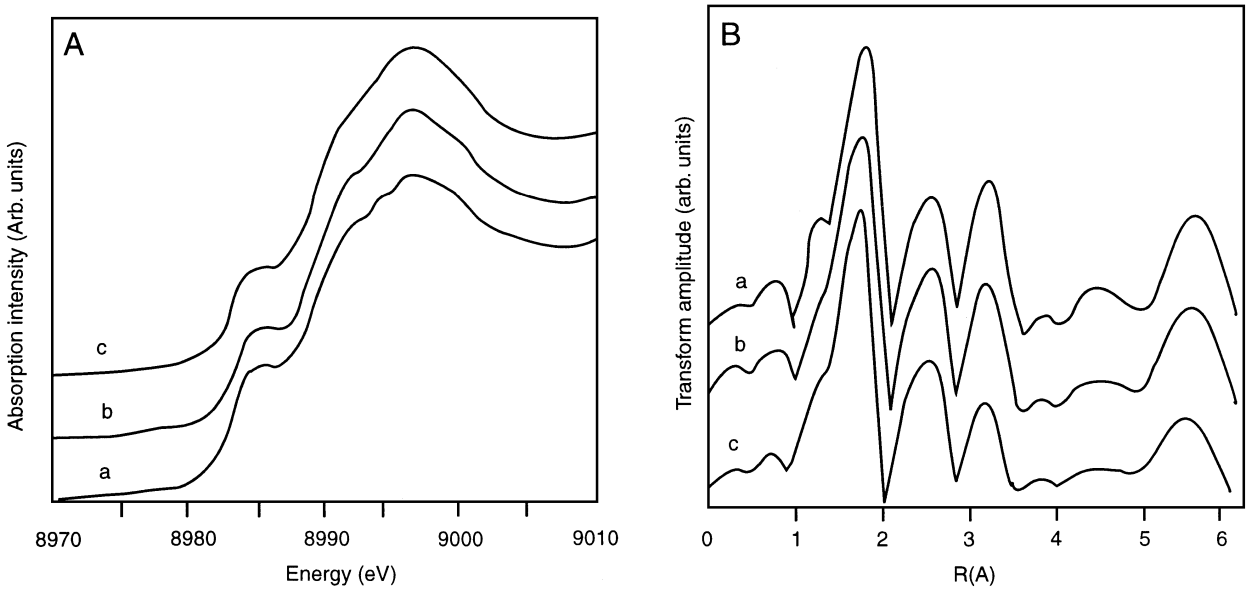

FIG. 6. Cu *K*-edge absorption spectra and Fourier transforms of the Cu EXAFS (B) of (a) model CuO, (b) calcined binary catalyst (CZ03) with Cu/Zn = 67/33, and (c) calcined ternary catalyst (CZA04) with Cu/Zn/Al = 60/30/10.

TABLE 2

Curve-Fitting Results of Cu and Zn EXAFS for the Calcined Catalysts

	Cu EXAFS			Zn EXAFS		
Catalyst		*R* (Å)	*N*		*R* (Å)	*N*
CZ03	Cu–O	1.96	4.5	Zn–O	1.97	4.5
				Zn–Zn	3.23	11.5
CZA04	Cu–O	1.96	4.4	Zn–O	1.97	4.4
				Zn–Zn	3.23	8.6

and model CuO. It is found that they are essentially the same. The first near-neighbor peaks for the catalysts in the Cu EXAFS results (shown in Fig. 6B) coincide with the peak from the four nearest-neighbor oxygen atoms in CuO. Curve-fitting results (listed in Table 2) show that both the binary and the ternary catalysts gave a Cu–O bond length of 1.96 Å and a coordination number of about 4.5 oxygen atoms. These values are close to the local structural parameter of CuO (two Cu–O bonds of 1.95 Å and two bonds of 1.96 Å). Furthermore, we can find from Fig. 7A that the Zn absorption *K*-edges for the binary and ternary catalyst and model ZnO exhibited essentially the same features too. The Fourier transformed Zn EXAFS of the catalyst is shown in Fig. 7B, and curve-fitting results are given in Table 2. It is found that the first near-neighbor peaks of both binary and ternary catalysts are also consistent with the peak from the Zn–O pair in ZnO (one ZnO bond of 1.99 Å and three bonds of 1.97 Å). These XAS and EXAFS results indicate that Cu was present as CuO and Zn was present as ZnO in both the binary and the ternary catalyst.

By comparing the second and third near-neighbor peaks of Cu EXAFS, it can be found that their corresponding positions were the same, while their intensities were slightly reduced for the catalysts, especially for the ternary catalyst. In the Zn EXAFS, ZnO exhibites a particularly intense second-shell peak at about 2.8 Å due to 6 Zn at 3.21 Å and 6 Zn at 3.25 Å. However, the peaks at about 2.8 Å for the calcined catalyst are much smaller. Curve-fitting results show that the coordination number for the peaks of binary and ternary catalysts are 11.5 and 8.6, respectively. All of these differences in the structure features of the *K*-edge absorption and fitted EXAFS results between binary, ternary, and CuO indicate that there were some differences in the local surroundings between the catalysts and those well-crystallized CuO.

In Fourier transforms of the Cu EXAFS for calcined catalyst (Fig. 6B), an unnegligible scatter peak at 3.09 Å was present and it seems to be ascribed to the Cu–Zn scattering of the catalyst just as previously suggested (42). According to this result, Sankar (42) believed that the calcined catalysts contained two copper species, Cu^{2+} in a CuO-like phase and Cu^{2+} occupying substitutional sites in the ZnO lattice. However, it is unfortunate that in our experiment, the backscatter peak at 3.09 Å was also present for the model CuO. Therefore, we cannot obtain the conclusion that some of the copper species were substituted in the ZnO lattice. In fact, both XAS and EXAFS results of Cu and Zn *K*-edge show that, in the calcined catalysts, copper existed mainly as separate microcrystallite CuO particles,

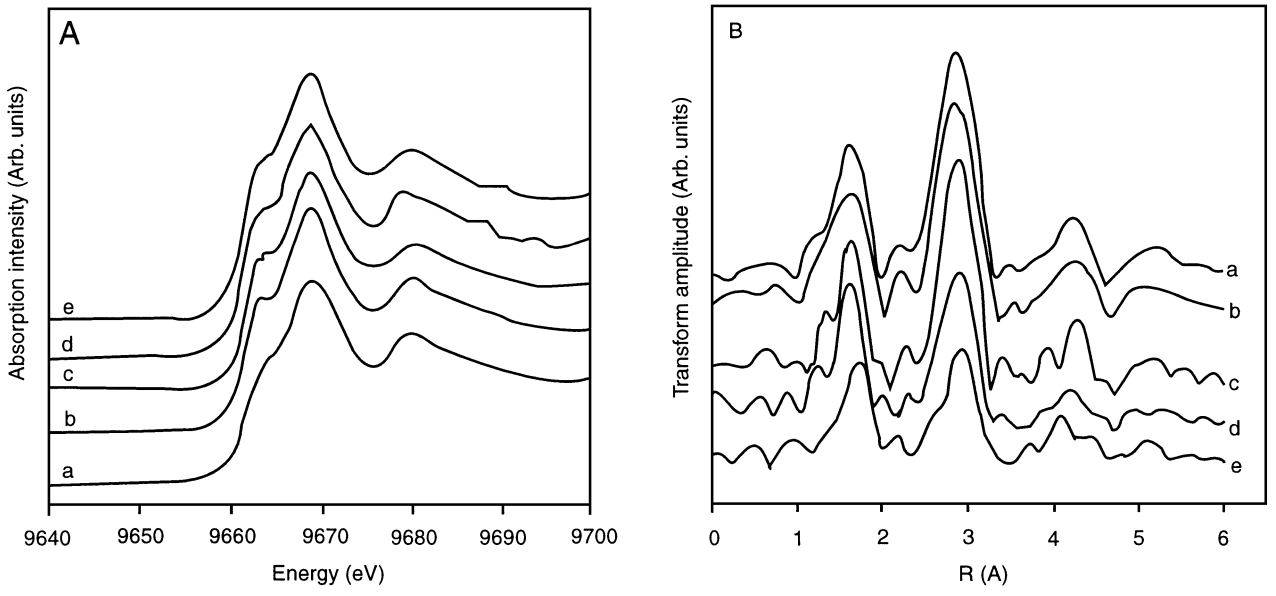

FIG. 7. Zn *K*-edge absorption spectra (A) and Fourier transforms of the Zn EXAFS (B) of (a) model ZnO, (b) calcined binary catalyst (CZ03) with Cu/Zn = 67/33, (c) calcined ternary catalyst (CZA04) with Cu/Zn/Al = 60/30/10, (d) reduced binary catalyst (CZ03) with Cu/Zn = 67/33, and (e) reduced ternary catalyst (CZA04) with Cu/Zn/Al = 60/30/10.

while zinc existed as separate ZnO particles. The EXAFS reveals that the addition of Al to a CuO–ZnO binary system prevented the formation of any ordered zinc phase and made the copper and zinc in catalyst appear in much smaller crystallites and exhibit an amorphous-like or less well-ordered structure feature. This is in agreement with the XRD results mentioned above and reported previously (43) and is approximately the same as the EXAFS results reported by Clausen *et al.* (44).

Characterization of Reduced Catalysts

When the ternary $Cu/ZnO/Al_2O_3$ catalysts were reduced by an $H_2/Ar(5/95)$ mixture at 240°C, it can be found from Fig. 8 that XRD lines for CuO were absent for the reduced sample while diffraction lines for Cu^0 were present. This indicates that CuO in the ternary $CuO/ZnO/Al_2O_3$ was completely reduced to metallic copper. The mean crystallite sizes were determined using the Scherrer equation, $d = k\lambda/\beta\cos\theta$, and the results are listed in Table 3. This shows that the mean crystallite size of ZnO was smaller than that of the metallic copper and that it increased with the increase of zinc content. The mean particle sizes of metallic copper determined by X-ray diffraction are consistent with those calculated by the specific area of metallic copper determined by N_2O decomposition over metallic copper (see Table 3). No spinel $CuAl_2O_4$ phase is found in Fig. 8. The diffraction lines of Cu and ZnO are broadened, especially at lower Cu content, suggesting that Cu atoms were highly dispersed and exhibited "X-ray amorphous" features due to the formation of amorphous and/or microcrystallites during reduction. Klier *et al.* (13, 45) have also observed the broadening or the absence of X-ray diffraction lines and suggested that Cu was highly dispersed and a considerable amount of amorphous phase was formed. It is consistent with our observations.

TABLE 3

Properties of Reduced Ternary and Binary $Cu/ZnO/Al_2O_3$ Catalysts

Catalysts	Composition Cu/Zn/Al (at.%)	Metallic copper surface area (N_2O) ($m^2 \cdot g^{-1}$)	Copper metal crystallite size (XRD) (nm)	ZnO crystallite size (XRD) (nm)	Copper metal crystallite size (N_2O)[a] (nm)
CZA01	10/80/10	5.8	<7.9	8.4	11.5
CZA02	30/60/10	19.1	7.9	6.3	10.5
CZA03	45/45/10	28.8	10.7	5.5	10.5
CZA04	60/30/10	36.3	10.7	3.9	11.0
CZA06	80/10/10	38.5	14.3	3.6	13.9
CZ02	50/50/0	6.9	46.8	16.3	48.5

[a] $d_{Cu}(N_2O)$ was calculated from specific surface area of metallic copper with a spherical particle model.

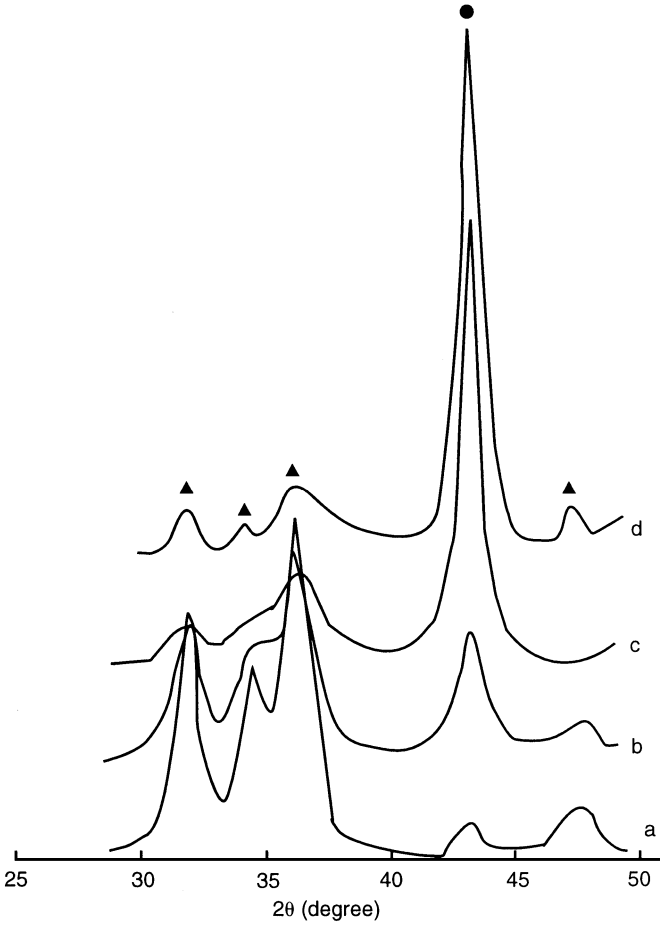

FIG. 8. XRD of the reduced $Cu/ZnO/Al_2O_3$ catalysts. (a) CZA01(10/80/10); (b) CZA02(30/60/10); (c) CZA04 (Cu/Zn/Al = 60/30/10); (d) CZA06 (Cu/Zn/Al = 80/10/10). (▲) ZnO; (●) Cu.

Photographs of the transmission electron microscope of the reduced catalysts with various composition are shown in Fig. 9. These show that the reduced catalysts consisted of clusters of interconnected particle with sizes of 10–15 nm. The fine ZnO particles adhere to the surface of metallic copper, hence the sintering of copper particles was obstructed. It was observed that the particle sizes of metallic copper increased with the increase of copper content. This is in agreement with the results from XRD and metallic copper surface area measurement. At a lower Cu content (see Figs. 9a and 9b), the copper particles were isolated and form spherical particles. At a higher Cu content (see Figs. 9c and 9d), the copper particles were agglomerated into clusters larger than 25 nm in size, but the metallic copper was still highly dispersed.

Figure 10A shows the X-ray absorption edge spectra of the reduced binary and ternary catalysts and model Cu and Cu_2O. By comparing Figs. 6A and 10A, it is found that absorption edge shifted to lower energy after reduction of the calcined catalysts and there is essentially no difference in the structure and position of *K*-edges between the

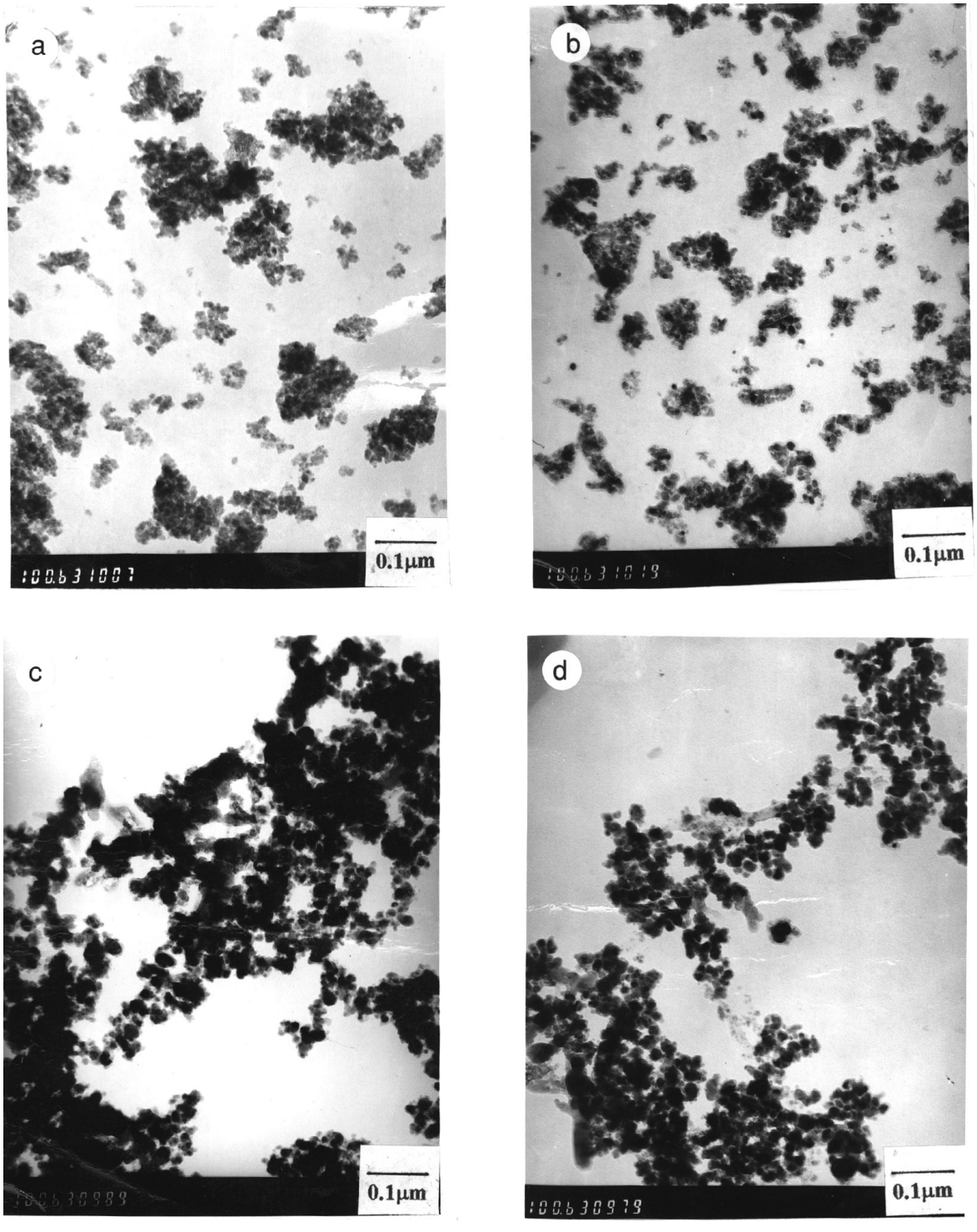

FIG. 9. TEM of the reduced Cu/ZnO/Al_2O_3 catalysts. (a) CZA01 (Cu/Zn/Al = 10/80/10); (b) CZA02 (Cu/Zn/Al = 30/60/10); (c) CZA04 (Cu/Zn/Al = 60/30/10); (d) CZA06 (Cu/Zn/Al = 80/10/10).

reduced catalysts and metallic copper, while there is a remarkable discrepancy between Cu_2O and the reduced catalysts. This indicates that the copper in the catalysts was reduced to metallic copper. This is further supported by the Cu EXAFS results. Figure 10B shows the Fourier transformed Cu EXAFS of reduced binary and ternary catalysts and metallic copper. The only strong peaks for reduced catalysts and metallic copper are the backscatter peaks at 2.55 Å corresponding to the Cu–Cu first coordination shell feature. The reduction in peak amplitude for the reduced

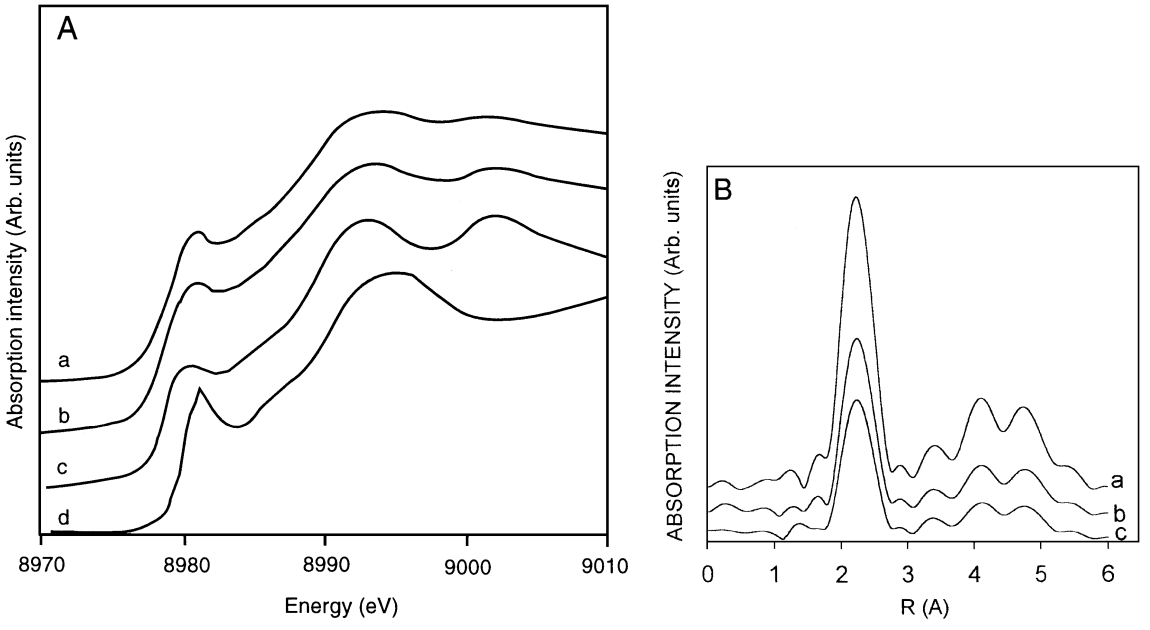

FIG. 10. Cu *K*-edge absorption spectra (A) and Fourier transforms of the Cu EXAFS (B) of (a) reduced CZA04 catalyst with Cu/Zn/Al = 63/30/10; (b) reduced CZ03 catalyst with Cu/Zn = 2/1; (c) model metallic copper; and (d) model Cu_2O.

catalysts indicates that copper was highly dispersed in the catalysts. Curve-fitting results (listed in Table 4) show that the Cu–Cu first coordination number is 7.0 in the reduced binary catalyst and 6.0 in the reduced ternary catalyst. The values are much less than 12 as is expected in bulk copper. The smaller Cu–Cu first coordination number for the reduced catalyst reveals that some amorphous-like copper existed in the reduced catalyst and the Cu in the reduced ternary catalyst was present in a much smaller Cu cluster than in the binary system. This part of amorphous-like copper could not be detected by XRD.

Figure 8 shows that only X-ray diffraction peaks of metallic copper and ZnO phases were present for the reduced catalysts while no diffraction line of metallic zinc ($2\theta = 42.4^\circ$) was observed. Furthermore, by analyzing and comparing Figs. 7A and 7B and the curve-fitting results (see Tables 3 and 4), we also find that there is no observable variation in the structural features of Zn *K*-edge absorption and fitted EXAFS results between model ZnO and reduced binary and ternary catalysts. In addition, there was no backscatter peak at about 2.32 Å corresponding to Zn–Zn first coordination shell feature. According to the results above, it can be concluded that no ZnO in the catalysts was reduced to Zn under the reduction condition. However, the backscatter peaks at about 2.8 Å and the coordination number of more distant coordination shell of the reduced catalyst are smaller than those of the calcined catalyst, and those of reduced ternary catalyst are smaller than those of the reduced binary catalyst.This indicates that ZnO was further dispersed and much smaller crystallites and amorphous-like structures were formed after reduction and addition of Al. This is in agreement with previous observations by X-ray diffraction (13, 25, 45) and EXAFS (24).

TABLE 4

Curve Fitting Results of Cu and Zn EXAFS for the Reduced Catalysts

	Cu EXAFS		Zn EXAFS		
Catalyst	*R* (Å)	*N*		*R* (Å)	*N*
CZ03	2.55	7.0	Zn–O	1.98	4.1
			Zn–Zn	3.22	10.0
CZA04	2.55	6.0	Zn–O	1.96	4.3
			Zn–Zn	3.22	7.9

Effect of the Composition and Copper Surface Area of the Catalyst on the Catalytic Activity

The catalytic activity and selectivity to methanol for methanol synthesis on the catalysts with various compositions are listed in Table 5. Comparing the $Cu/ZnO/Al_2O_3$ ternary catalysts with the binary Cu/ZnO catalysts, it can be found that the former shows a higher conversion of CO_2 and higher yield of methanol. This can be attributed to the fine particle size of metallic copper and higher copper metal surface area in the ternary catalyst. In addition, the catalytic activity of the $Cu/ZnO/Al_2O_3$ ternary catalyst increased with the increase of Cu/Zn ratio until it reached a maximum at a Cu/Zn ratio of 1–2.

To avoid the influence of the limitation of the thermodynamic equilibrium on the catalytic activity results of the

TABLE 5

Performance of Methanol Synthesis from $CO_2 + H_2$ over Various Catalysts[a]

Catalyst	Composition Cu/Zn/Al (at.%)	Reaction temperature (°C)	CO_2 conversion (%)	CO selectivity (%)	MeOH selectivity (%)	MeOH yield (%)	TOF of MeOH[b] $\cdot 10^3$ (s^{-1})
CZ01	30/70/0	220	5.9	52.5	47.5	2.8	2.58
		240	12.4	68.4	31.6	3.6	3.31
		260	17.2	80.8	19.2	3.3	3.04
CZ02	50/50/0	220	7.7	57.2	42.8	3.3	2.20
		240	13.9	65.5	34.5	4.8	3.20
		260	18.3	81.4	18.6	3.4	2.27
CZ03	60/30/0	220	7.2	54.8	45.2	3.3	1.13
		240	12.2	63.9	36.1	4.4	1.50
		260	18.2	77.5	22.5	4.1	1.40
CZA01	10/80/10	220	4.6	51.3	48.7	2.3	2.03
		240	11.1	69.2	30.8	3.4	3.00
CZA02	30/60/10	220	10.4	58.1	41.9	4.4	1.18
		240	17.0	71.3	28.7	4.9	1.31
CZA03	45/45/10	220	15.5	57.9	42.1	6.5	1.15
		240	19.3	66.7	33.3	6.4	1.14
CZA04	60/30/10	220	14.7	53.3	46.7	6.9	0.97
		240	16.8	64.2	35.8	6.0	0.85
CZA06	80/10/10	240	16.1	69.8	30.2	4.9	0.65

[a] Reaction conditions: $P = 2.0$ MPa, SV $= 3600\ h^{-1}$, $CO_2/H_2 = 1/3$ (molar ratio).

[b] $TOF_{CH_3OH} = \dfrac{\text{Formed molecular number of methanol } (N)}{\text{time(S)} \cdot \text{number of metallic copper atom } (N)} = \dfrac{\left(\text{Yield}_{CH_3OH}\,\% \cdot SV \cdot 1/4 \cdot 6.02 \times 10^{23}\right)/22.4}{3600 \cdot S_{Cu} \cdot 1.46 \times 10^{19}} (N_{CH_3OH} \cdot N_{Cu}^{-1} \cdot s^{-1})$.

ternary Cu/ZnO/Al_2O_3 catalyst, a catalytic activity test was also carried out under higher hourly space velocity (i.e., 25,000 h^{-1}) and the results are shown in Fig. 11. It can be found that the yield of methanol reached a maximum at about 60% copper content. The difference of the optimized composition between our results and the literature's reports (13, 46–48) is due to the difference of the preparation method, as it has been proposed that the optimized composition is related to the preparation method (46). For example, with the ternary Cu/ZnO/Al_2O_3 catalyst, the novel gel oxalate coprecipitation method derived an optimized composition of about Cu/Zn ratio of 1–2, 10 Al%. This is consistent with the results obtained by acetate rout (47) as well as those of commercial catalyst prepared by conventional carbonate coprecipitation (6). The most favorable copper content of a Raney catalyst (39) is 97% (after extraction) obtained from a CuZnAl alloy of composition 30–36/20–14/50%. For the binary Cu/ZnO catalyst, the conventional carbonate coprecipitation gave an optimized composition of Cu/Zn = 3/7 (13). However, our results show that the best composition is about Cu/Zn = 1/1.

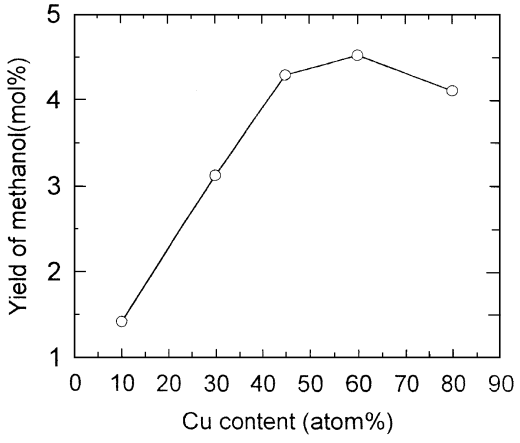

FIG. 11. Effect of Cu concentration of the ternary catalyst on yield of CH_3OH at 240°C, 2.0 MPa, and hourly space velocity of 25000 h^{-1}; $CO_2/H_2 = 1/3$ (molar ratio).

Various compositions and different preparation methods of Cu-containing catalysts can strongly influence their catalytic activity for methanol synthesis. It has been proposed (30–33) that the yield of methanol is directly proportional to the surface area of metallic copper for Cu/ZnO/Al_2O_3 or supported copper catalysts in the synthesis of methanol from the hydrogenation of CO/CO_2. However, there are also conflicting reports (7, 49, 50) which suggest that the yield of methanol is not proportional to the surface area of metallic copper for the Cu/ZnO and Cu/ZnO/Al_2O_3 catalysts. There are fewer studies on the relations of catalytic activity for methanol synthesis from hydrogenation of CO_2 to the surface area of metallic copper.

In our experiment, the effect of the surface area of metallic copper on the activity of synthesis of methanol from the hydrogenation of CO_2 over Cu/ZnO/Al_2O_3 catalysts was studied at different SV and the results are shown in Fig. 12. It can be seen that the catalytic activity increased with the

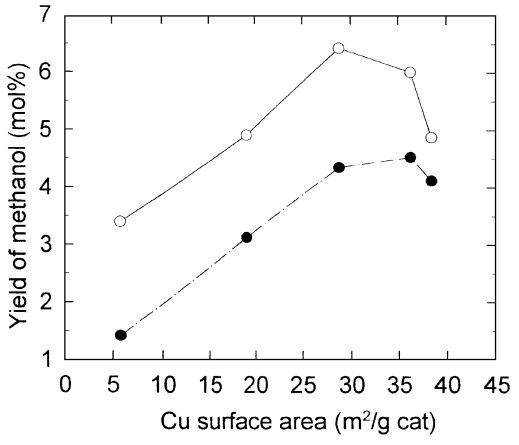

FIG. 12. The relationship between the yield of CH_3OH and Cu specific surface area at 240°C, 2.0 MPa, and hourly space velocity of (●) 3,600 h^{-1} and (○) 25,000 h^{-1}.

increase of the surface area of metallic copper, but it was not a linear relationship. The catalytic activity at 60% of copper content (Cu surface area is 36.3 m^2/g) deviated from the linear trend of variation of the activity within 10–45% of the copper contents (corresponding to Cu surface area of 5.8–28.8 m^2/g) and decreased at 80% of the copper content though the copper surface area is the largest (38.5 m^2/g). This indicates that the catalytic activity of the catalysts depends on both the metallic copper surface area and the powerful synergy between copper and zinc oxide.

In order to further clarify this point, we calculated the TOF (turnover frequency, which means *formed molecular number of methanol per second per metallic copper atom*) of methanol formation over various catalysts according to the literature (51, 52). The TOF results are listed in Table 5 and are also plotted versus metallic copper surface area (shown in Fig. 13). It is important to note that the TOF of methanol formation decreased with the increase of metallic copper

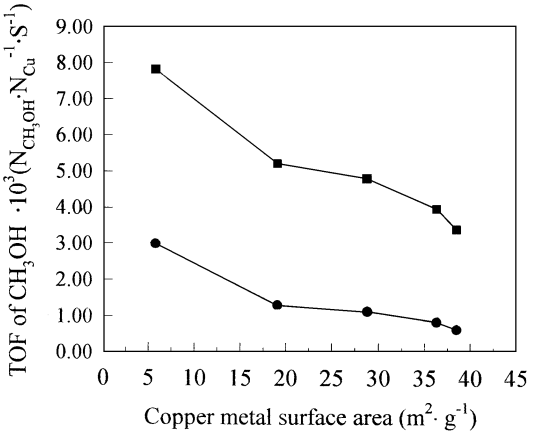

FIG. 13. The relationship between the TOF of methanol formation and Cu specific surface area at 240°C, 2.0 MPa, and hourly space velocity of (●) 3,600 h^{-1} and (■) 25,000 h^{-1}.

surface area under different hourly space velocity. According to Boudart's theory (51, 52), if the catalytic activity of the catalyst only depends on the metallic copper surface area, then the plot of TOF versus metallic copper surface area should be a horizontal line. However, TOF of methanol formation decreased with the increase of metallic copper surface area as shown in Fig. 13, which indicates that the catalytic activity for methanol synthesis not only depends on the metallic copper surface area but also on the interaction between copper and zinc oxide (that could be a powerful synergy). This means that the interaction between copper and zinc oxide promoted the catalytic properties of the catalysts for methanol synthesis. This could be ascribed to the fact that when the concentration of the copper was lower, the fractions of microcrystalline or amorphous-like CuO were relatively higher. In this kind of structure, some of the copper species are incorporated substitutionally in the ZnO lattice. This point has been demonstrated vigorously by previous EXAFS (24, 42) and XPS (29) results though we did not carry out the detailed research in this paper. However, in our detailed study on the surface structure of $Cu/ZnO/Al_2O_3$ catalysts and chemical state of copper by *in situ* XPS has also provided much identical evidence (53). The Cu^{2+} ion in the ZnO lattice has a slightly distorted tetrahedral symmetry (54, 55) (while in the case of CuO, the Cu^{2+} ion is surrounded by four oxygen ions in a nearly square-planar symmetry (29). Thus, it led to the changes of coordination environment and electronic properties of Cu and Zn atoms in the catalyst. This change is exhibited as a powerful syngergy which benefited the methanol synthesis. In addition, it is also noteworthy in Table 3 that the Cu^0 crystallite size determined by N_2O-decomposition adsorption method seems to be about the same in all of the $Cu/ZnO/Al_2O_3$ catalyst. Surprisingly, the Cu^0 crystallite size of the catalyst containing 10% copper (molar ratio) seems to be larger than that of the catalysts containing 20–45% copper. This is because for the catalysts containing lower copper content, some of the copper was incorporated substitutionally in the ZnO lattice. However, only microcrystalline copper species can be detected by XRD or N_2O-decomposition adsorption while the copper species incorporated in the ZnO lattice cannot be done. As a result, the Cu^0 crystallite size calculated according to the metallic copper surface area determined by N_2O-decomposition adsorption method using the spherical model could be larger than the real values. However, when the concentration of copper exceeds the maximum, a considerable amount of copper species was present mainly in relative well-ordered crystalline and larger particle size CuO, and the synergy was weakened, so the catalytic activity decreased slightly.

Effect of Reaction Condition on Catalytic Behavior

The variation of catalytic activity for methanol synthesis with different temperatures shown in Fig. 14 reveals that the

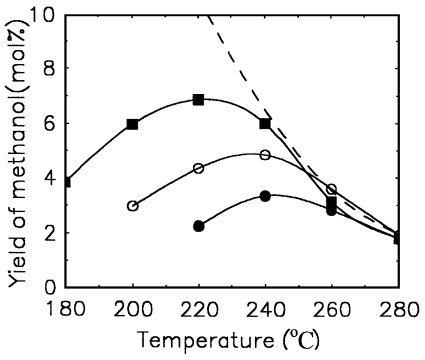

FIG. 14. Effect of temperature on the catalytic activity of methanol synthesis at 2.0 MPa, space velocity of 3600 h^{-1} on catalysts: (●) CZA01; (○) CZA02; (□) CZA04; (– – –) calculated formation rate of methanol based on thermodynamic equilibrium.

yield of methanol has a maximum. It is well known that the rate of reaction increases with the increase of temperature kinetically, so the yield of methanol should increase with the increase of temperature. However, the yield of methanol declines with the increase of temperature due to the limitation of the thermodynamic equilibrium. Therefore, it can be concluded from the existence of the maximum yield of methanol that the control factor of the reaction transforms from kinetics to thermodynamics. The maximum yield of methanol should be reached at a lower temperature if a catalyst is active enough. We can see from Fig. 14 that the maximum is obtained at 220°C for the highly active catalyst (CZA04) and at 240°C for the lower active catalysts (CZA01, CZA02). Because of the limitation of the thermodynamic equilibrium, the yields of methanol for various catalysts under higher temperature conditions are close to the yields of methanol for thermodynamic equilibrium.

In order to clarify whether methanol is produced directly by carbon dioxide hydrogenation or via the intermediate formation of carbon monoxide, the influence of the contact time (reciprocal of space velocity) on the methanol selectivity was investigated (as shown in Fig. 15). It is well known that the reverse water gas-shift reaction (RWGS) and methanol synthesis reaction coexist in carbon dioxide hydrogenation presented as (56)

$$\mathrm{CO_2(g) + 3H_2(g) = CH_3OH(g) + H_2O(g)}$$
$$\Delta H_{298} = -49.47\ \mathrm{kJ \cdot mol^{-1}}$$
$$\Delta G_{298} = 3.30\ \mathrm{kJ \cdot mol^{-1}} \qquad [1]$$

$$\mathrm{CO_2(g) + H_2(g) = CO(g) + H_2O}$$
$$\Delta H_{298} = 41.17\ \mathrm{kJ \cdot mol^{-1}}$$
$$\Delta G_{298} = 28.64\ \mathrm{kJ \cdot mol^{-1}}. \qquad [2]$$

Carbon monoxide is an unavoidable intermediate precursor. If the catalyst is highly active and the contact time of reaction gas with the catalyst is long enough, the decomposition of methanol (produced in reaction [1]) or the hydrogenation of carbon monoxide (produced in reaction [2]) will take place. The possible secondary reaction is

$$\mathrm{CH_3OH \rightleftharpoons CO + 2H_2} \qquad \Delta H_{298} = 90.64\ \mathrm{kJ \cdot mol^{-1}}$$
$$\Delta G_{298} = 25.34\ \mathrm{kJ \cdot mol^{-1}}. \qquad [3]$$

The selectivity to methanol (S) and relative selectivity (γ) are presented in Fig. 15as functions of the contact time (τ) for CZA04 catalyst. Both curves tend toward the finite values as the contact time τ approaches zero, suggesting that parallel routes to methanol and carbon monoxide exist under enough high hourly space velocity condition. However, it is noted that the selectivity to methanol increases and selectivity to carbon monoxide decreases with the increase of the space velocity. It is well known that, if both carbon monoxide and methanol are formed merely from primary reaction simultaneously, the ratio of selectivity to methanol and carbon monoxide will remain constant with the change of the space velocity. The decreasing of selectivity to methanol and the increasing of that to carbon monoxide with the decreasing of the space velocity indicates that part of the carbon monoxide is formed from the secondary reaction under our experimental conditions. This is because when the gas hourly space velocity is low (or the contact time of reaction gas with the catalyst surface was long), secondary reaction of methanol decomposition or hydrogenation of carbon monoxide (reaction [3]) will be an unnegligible process. The increasing of selectivity to CO indicates that the methanol decomposition could be a major secondary reaction. As a result, the decreasing of selectivity to methanol and the increasing of that to CO were found with the decreasing of the gas hourly space velocity. In other words, only methanol and CO were primary products when the gas hourly space velocity was high enough;

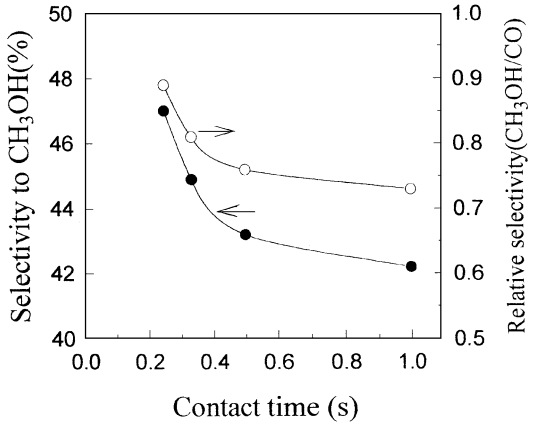

FIG. 15. Carbon dioxide hydrogenation over Cu/ZnO/Al_2O_3 ternary catalyst (CZA04). Variation of (○) relative selectivity $\gamma = x(\mathrm{CH_3OH})/x(\mathrm{CO})$($x$ = molar fraction) and (●) selectivity to methanol as a function of the catalyst mass-related contact time τ[s]. Conditions: $\mathrm{CO_2/H_2}$ = 1/3(molar ratio), 220°C, 2.0 MPa.

the contact time of reaction gas with the catalyst surface was short enough and all of the secondary process were depressed completely. This indicates that methanol and CO can be formed via reactions [1] and [2] simultaneously. From the analysis above, it can be concluded that the formation of methanol is a primary process of reaction [1]. The methanol formation from hydrogenation of carbon monoxide (reaction [3]) formed from the reverse water gas shift reaction is negligible. Some previous kinetic studies (15) suggest that methanol and carbon monoxide are formed by parallel routes from carbon dioxide. From radiotracer studies using a $Cu/ZnO/Al_2O_3$ catalyst under industrial conditions, Chinchen *et al*. (6) suggest that methanol synthesis proceeds from carbon dioxide, even in the presence of carbon monoxide. Koeppel and Baiker (57) conclude from the investigation of the influence of the residence time on the relative rate of product formation (CH_3OH, CO) using Cu/ZrO_2 catalyst that methanol is formed from carbon dioxide via a reaction pathway parallel to that of the formation of gaseous carbon monoxide, possibly via a common surface intermediate. These conclusions are basically consistent with ours.

CONCLUSIONS

$Cu/ZnO/Al_2O_3$ catalysts with fine particles, high surface area, and high activity for synthesis of methanol from CO_2 hydrogenation have been prepared by the novel oxalate gel coprecipitation method. Copper, zinc, and aluminum were coprecipitated and isomorphous substituted oxalates were formed. The addition of Al led to a decrease in crystallite sizes of the catalyst, prevented the formation of any ordered zinc phase, and made the copper and zinc in the catalyst exhibit amorphous-like or less well-ordered structure features.

The optimized composition is $Cu/Zn = 1–2$, 10% Al. The catalytic activity increases with the increase of the copper content below 80%. The yield of methanol increases with the increase of specific area of metallic copper, but it is not a linear relationship. This indicates that the synergy for the synthesis of methanol exists between copper and zinc oxide. The selectivity of methanol increases with the increase of space velocity, suggesting that methanol is the primary product and is formed directly from $CO_2 + H_2$. The secondary process of hydrogenation of carbon monoxide via the route of the reverse water–gas shift reaction is not significant for methanol synthesis from CO_2 hydrogenation.

ACKNOWLEDGMENTS

This work was supported by the National Foundation of Natural Sciences and the Foundation of State Key Laboratory of Coal Conversion. The authors are grateful for the support of National Laboratory of High Energy Physics (KEK, Tsakuba, Japan) in the XAS/EXAFS experiment.

REFERENCES

1. Badiische Anilin and Soda Fabrik, German Patents 415, 686, 441, 443, 462, and 837 (1923); US Patents 1,558,559 and 1,569,755 (1923).
2. Kotowski, W., *Chem. Tech.* **15**, 204 (1963).
3. Davis, P., Snowdon, F. F., Bridger, G. W., Hughes, D. O., and Young, P. W., UK Patent 1010871 (1965).
4. Collins, B. M., UK Patent 140512 (1975).
5. Brown Bourzutschky, J. A., Homs, N., and Bell, A. T., *J. Catal.* **124**, 73 (1990).
6. Chinchen, G. C., Denny, P. J., Parker, D. G., Spencer, M. S., and Whan, D. A., *Appl. Catal.* **30**, 333 (1987).
7. Klier, K., Chatikavanij, V., Herman, R. G., and Simmons, G. W., *J. Catal.* **74**, 343 (1982).
8. Liu, G., Willcox, D., Garland, M., and Kung, H. H., *J. Catal.* **90**, 139 (1984).
9. Kieffer, R., Ramarson, E., Deluzarche, A., and Trambouze, Y., *Rect. Kinet. Catal. Lett.* **16**, 207 (1981).
10. Denise, B., Sneeden, R. P. A., and Hamon, C., *J. Mol. Catal.* **17**, 359 (1982).
11. Chinchen, G. C., Denny, P. J., Parker, D. G., Short, G. D., Spencer, M. S., Waugh, K. C., and Whan, D. A., "ACS Division of Fuel Chemistry," Vol. 29, No. 5, p. 178. Am. Chem. Soc., Washington, DC, 1984.
12. Rozovskii, A. Ya., Lin, G. T., Liberov, L. G., Slivinskii, E. V., Loktev, S. M., Kagan, Y. B., and Bashkirov, A. N., *Kinet. Catal.* **18**, 691 (1977).
13. Herman, R. G., Klier, K., Simmons, G., Finn, B. P., Bulko, J. W., and Kobylinski, T. P., *J. Catal.* **56**, 407 (1979).
14. Klier, K., *Adv. Catal.* **31**, 243 (1982).
15. Rozovskii, A. Ya., *Kinet. Catal.* **21**, 78 (1980).
16. Liu, G., Willcox, D., Garland, M., and Kung, H. H., *J. Catal.* **96**, 251 (1985).
17. Jackson, S. D., *J. Catal.* **115**, 247 (1989).
18. Duprez, D., Fevhat-Hamida, Z., and Bettahar, M. M., *J. Catal.* **124**, 1 (1990).
19. Chanchlani, K. G., Hudgins, P. R., and Silveston, P. L., *J. Catal.* **136**, 59 (1992).
20. Vedage, G. A., Pitchai, R., Herman, R. G., and Klier, K., *in* "Proceedings, 8th International Congress on Catalysis, Berlin, 1984," Vol. II, p. 47. Dechema, Frankfurt-am-Main, 1984.
21. Inui, T., and Takeguchi, T., *Catal. Today* **10**, 95 (1991).
22. Nonneman, L. E. Y., and Ponet, V., *Catal. Lett.* **7**, 213 (1990).
23. Okamoto, Y., Konishi, Y., Fukino, K., Imanaka, T., and Teranishi, S., *in* "Proceedings, 8th International Congress on Catalysis, Berlin, 1984," p. V-159. Dechema, Frankfurt-am-main, 1984.
24. Kau, L., Hodgson, K. O., and Solomon, E. I., *J. Am. Chem. Soc.* **111**, 7103 (1989).
25. Bulko, J. B., Herman, R. G., Klier, K., and Simmons, G. W., *J. Phys. Chem.* **83**(24), 3118 (1979).
26. Monnier, J. R., Hanrahan, M. J., and Apai, G., *J. Catal.* **92**, 119 (1985).
27. Apai, G., Monier, J. R., and Preuss, D. R., *J. Catal.* **98**, 563 (1986).
28. Parris, G. E., and Klier, K., *J. Catal.* **97**, 374 (1986).
29. Okamoto, Y., Fukino, K., Imanaka, T., and Teranishi, S., *J. Phys. Chem.* **87**, 3747 (1983).
30. Chinchen, G. C., Waugh, K. C., and Whan, D. A., *Appl. Catal.* **25**, 101 (1986).
31. Denise, B., Sneeden, R. P. A., Beguin, B., and Cherifi, O., *Appl. Catal.* **30**, 353 (1987).
32. Chinchen, G. C., and Waugh, K. C., *J. Catal.* **97**, 280 (1986).
33. Fleisch, T. H., and Mieville, R. L., *J. Catal.* **90**, 165 (1984).
34. Bridgewater, A. J., Wainwright, M. S., and Young, D. J., *Appl. Catal.* **28**, 241 (1986).
35. Frost, J. C., *Nature* **334**(18), 577 (1988).
36. Deng, J. F., Sun, Q., and Zhang, Y. L., *Appl. Catal. A* **139**, 75 (1996).
37. Chinchen, G. C., Hay, C. M., Vandervell, H. D., and Waugh, K. C., *J. Catal.* **103**, 79 (1987).

38. Friedrich, J. B., Wainwaight, M. S., and Young, D. J., *J. Catal.* **80**, 1 (1983).
39. Evans, J. W., Wainwright, M. S., Bridgewater, A. J., and Young, D. J., *Appl. Catal.* **7**, 75 (1983).
40. Chen, J., Lu, G., and Ma, L. D., *J. Fudan Univ. (Nature Science Chinese)* **28**, 78 (1989).
41. Butt, J. B., and Weekman, V. W., *AIChE Symp. Ser.* **70**, 27 (1974).
42. Sankar, G., Vasudevan, S., and Rao, C. N. R., *J. Chem. Phys.* **85**(4), 2291 (1986).
43. Gherardi, P., Ruggeri, O., Trifiro, F., Vaccari, A., del Piero, G., Manara, G., and Notari, B., *in* "Preparation of Catalysts III" (G. Poncelet, P. Grange, and P. A. Jacobs, Eds.), p. 723. Elesevier, Amsterdam, 1983.
44. Clausen, B. S., Lengeler, B., and Rasmussen, B. S., *J. Phys. Chem.* **89**, 2319 (1985).
45. Mehta, S., Simmons, G. W., Klier, K., and Herman, R. G., *J. Catal.* **57**, 339 (1979).
46. Bart, J. C. J., and Sneeden, R. P. A., *Catal. Today* **2**, 1 (1987).
47. Bardet, R., Thivolle-Cazat, J., Trambouze, Y., and Hamon, C., French Patent 2,529,098 (1983).
48. Andrew, S. P. S., *in* "Proceedings, 7th International Congress on Catalysis, Tokyo, 1980" (T. Seiyama and K. Tanabe, Eds.), Plenary Lecture (Paper 12) Post Congress Symposium, Elsevier, Amsterdam, 1981.
49. Burch, R., and Chappel, R. J., *Appl. Catal.* **45**, 131 (1988).
50. Berndt, H., Briehn, V., and Evert, S., *Appl. Catal. B* **86**, 65 (1992).
51. Boudart, M., and Diéga-Mariadassou, G., "Kinetics of Heterogenous Catalytic Reactions" (Translated by Zi Gao) Chinese ed., p. 144. Fudan Univ. Press, Shanghai, 1988.
52. Boudart, M., *Chem. Rev.* **95**, 661 (1995).
53. Sun, Q., Dai, W. L., Zhang, Y. L., and Deng, J. F., submitted for publication.
54. Dietz, R. E., Kamimura, H., Sturge, M. D., and Yariv, A., *Phys. Rev.* **132**, 1559 (1963).
55. Ketchik, S. V., Minyukova, T. P., Kuznetsova, L. I., Plyasova, I. M., Yurieva, T. M., and Boreskov, G. V., *React. Kinet. Catal. Lett.* **19**, 345 (1982).
56. Bridger, G. W., and Spencer, M. S., *in* "Catalyst Handbook" (M. V. Twigg, Ed.), p. 442. Wolfe Publishing, 1989.
57. Koeppel, R. A., and Baiker, A., *Appl. Catal. A* **84**, 77 (1992).